strain
An International Journal for Experimental Mechanics

In Situ Evaluation of Tensile Properties of Heat-Affected Zones from Welded Steel Pipes

G. M. Castelluccio*, A. A. Yawny[†‡], J. E. Perez Ipiña[‡§] and H. A. Ernst[¶]

*The George W. Woodruff School of Mechanical Engineering, Georgia Institute of Technology, Atlanta, GA 30332-0405, USA

[†]Grupo Física de Metales, Centro Atómico Bariloche (CNEA), Av. Bustillo 9500 (8400), Bariloche, Río Negro, Argentina

[‡]Consejo Nacional de Investigaciones Científicas y Técnicas (CONICET), Argentina

[§]Grupo Mecánica de Fractura, Universidad. Nacional del Comahue, Buenos Aires 1400 (8300), Neuquen, Neuquen, Argentina

[¶]Department of Structural Integrity, TENARIS Dr. Simini 250 (2804), Campana, Buenos Aires, Argentina

ABSTRACT: Currently, measuring the local tensile strength in inhomogeneous materials is not standardised, nor accepted techniques are available despite such technique would be beneficial in a variety of technological applications. Thus, this work introduces an innovative method for assessing stress–strain properties at a sub-millimeter scale and illustrates the potential of the technique by evaluating the strength of a sub-region in the HAZ from welded steels pipes. The method employs a fully instrumented stage inside a scanning electron microscope that stretches small tensile specimens (2.0 mm × 0.5 mm cross-section, 12.5 mm gage length) while registering detailed images of the deformed region. The specimens, cut from full-scale welds, include in their gage length weld metal, base metal and HAZ and have an 85 μm period grid of evaporated lead on their surface to visualise the deformation. Upon straining, local strain is determined by correlating sequential images of the specimen surface with an open source code for particle image velocimetry. The calculated local strain within the HAZ and the load values recorded during testing are converted into a local stress–strain response. The results for two different heat inputs agree with usual, but indirect and less accurate assessments procedures, including local hardness measurements and notched bar testing.

KEY WORDS: *HAZ, image correlation, inhomogeneity, in situ test, particle image velocimetry, steel pipe, tensile behaviour, weld small specimens*

Introduction

The structural integrity of offshore structures is a critical issue from economical and environmental points of view, and the safety of pipelines needs to be guaranteed during the installation and the operation. One economic procedure of laying offshore pipelines is the reeling process in which the pipeline undergoes back and forth plastic deformation up to 3% strain [1]. This severe deformation raises concerns about the possible detrimental impact on the integrity of the welds that join the pipes forming the pipeline. An in-depth structural reliability assessment of welded joints requires knowledge of strength and fracture toughness properties of the base metal, the weld metal and the region referred to as the heat-affected zone (HAZ). This region belongs to the base metal, but has different microstructures and properties as a result of the thermal cycle yielded by the heat input (HI) during the welding process. The heat affected material extends a few millimeters from the liquid–solid interface into the base metal and presents sub-regions with different grain sizes [2]. Of particular interest is the HAZ sub-region that borders the fusion line, the coarse-grain HAZ (CGHAZ), because it usually has the lowest toughness within the HAZ in HSLA steel [3], and pipeline standards require extensive and detailed characterisation of this sub-region [4]. Nevertheless, the characterisation of local mechanical properties of real HAZ microstructures presents intrinsic difficulties caused by the steep gradient of properties on a millimeter scale. As such small scale normally falls outside the scope of standardised tensile testing, strength-hardness correlations were suggested as an alternative to estimate of HAZ, but this approach can provide inaccurate results [5]. Therefore, there is still a need for developing adequate methodologies for the accurate characterisation of local HAZ mechanical properties.

The influence of chemical composition on tensile strength of HAZ material can be studied using thermo-mechanical simulators (such as the Gleeble technique, [6]), and results can provide useful information about phase transformations response of the microstructures associated to the HAZ (e.g. the volume fraction of Martensite). However, this technique can not reproduce all the features within the HAZ because it lacks weld passes, grain size gradients, weld mismatch and realistic residual stresses. In addition, a few studies characterised the tensile strength of HAZs using macroscopic specimens with multiple microstructures [7], but this technique do not differentiate individual sub-region behaviours. Moreover, other studies used micro-samples [8–10], but they neglected the gradients of properties within specimens of finite size, so they can not be used to study a specific sub-region interacting with the whole weld.

This work presents an innovative method for assessing the local stress–strain properties of small-scale microstructures, such as those associated to the different sub-regions of the HAZ in welding of steels pipes. The technique consists of testing small specimens inside a scanning electron microscope in conjunction with a computational strategy to assess strain fields from the registered images. The potential of the technique is illustrated by measuring the mechanical response of the CGHAZ from a girth weld of HSLA steel pipes. As production parameters such as the HI might influence the resulting properties, we applied the technique to assess on the effect of two different HIs, 0.8 and 2.5 KJ mm^{-1}, the stress–strain mechanical response of the CGHAZ. Additionally, we compared the results with those obtained from indirect assessments procedures such as local hardness measurements and notched bar testing.

doi: 10.1111/j.1475-1305.2010.00799.x

Experimental Details

Small-scale tests

This research studied the stress–strain properties on the sub-millimeter scale by means of mechanical tests inside a scanning electron microscope (SEM). Because of the wide depth of focus and magnification range provided by the SEM, *in situ* tests were appropriate for the study of mechanical properties on different scales. This technique allowed direct observation of the sample while it was being loaded and deformed inside a Philips 515 SEM, with the *in situ* stage in Figure 1. The stage had two mobile crossheads that served to stretch or compress specimens under displacement control. Furthermore, a linear variable differential transformer (LVDT) and a load cell measured the applied displacement and load, respectively. As the testing machine worked under the vacuum of the SEM chamber, access to the specimen was restricted during the test. For further details on the *in situ* stage, see ref. [11].

Specimens and material analysed

The SEM chamber has limited space inside, and only samples of restricted size fit in the stage, as shown in Figure 2. Moreover, the width of the sample depends on the maximum load sustained by the machine. The deformation attained in the sample was visible on a grid of squares drawn on the surface by laying a film of lead over a removable mask, typically employed to support material in transmission electron microscopy (TEM), with a diameter of 3 mm and a mesh 300, which is 300 lines per inch (85 μm of period). A close inspection of the surface assured that no debonding of lead occurred while it was stretched. Furthermore, the difference in atomic number between lead and iron provided an excellent contrast on SEM images. Similar solutions were proposed recently in the literature [12].

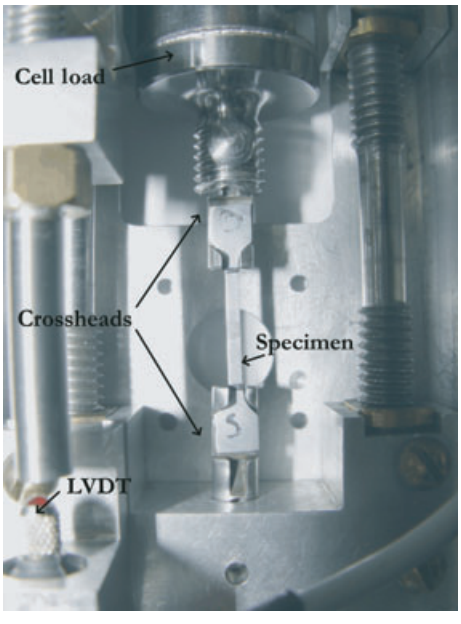

Figure 1: Photography of the testing machine with a tensile probe in place

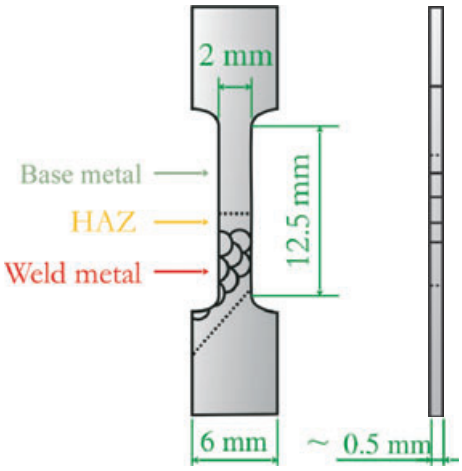

Figure 2: Small samples used for the in situ tests, cut from the centre part of the weld (cap and root were removed). Note the HAZ region along the straight bevel

To exemplify the capabilities of the method, we analysed the deformation of two HAZs from standard girth welds of an API X65 steel pipe for reeling applications. Table 1 presents the chemical composition extracted from industrial records, and Table 2 provides some basic mechanical properties of the X65 grade pipe obtained from standardised tests. A welding bevel with a straight side ('semi K bevel') was adequate in this study because the as-welded microstructural gradient within the HAZ lies in the axial direction [13]. Welding specifications included surface tension transfer (STT) technology from Lincoln Electric©, used for welding the root pass with a HI of HI_{root} = 0.8 KJ mm^{-1}. For the submerged arc welding (SAW) process used for the filling passes, we have considered in the present work two different HIs: 0.8 and 2.5 KJ mm^{-1}. In both cases, the strength of the weld metal was higher than that of the base metal, condition referred as overmatching (see Table 2 for HI 0.8 kJ mm^{-1}).

The loading axis of the specimens was in a transverse direction to the weld (note the weld in Figure 2), and it included some base metal, weld metal, and HAZ material, which are exemplified in the series of micrographs in Figure 3. The samples only contained material from the centre part of the weld (cap and root were removed by machining) because that is the region usually assessed by standards.

Deformation Measurements – Particle Image Velocimetry

Testing on a small scale requires developing new strategies for measuring the displacements and strains embedded in images. This physical information can be obtained from a myriad of mathematic tools; among the most common ones are Fourier analysis, wavelets, or simple correlations. The choice may depend on the physics of the problem (i.e., if some function is expected to describe the problem), previous background, or available tools. The analysis using a cross-correlation of images has been widely employed, and many commercial software applications are available to calculate the displacement field based on images.

doi: 10.1111/j.1475-1305.2010.00799.x

Table 1: Chemical composition (%) by weight of API grade X65 pipe material. Balanced with Fe

Al	C	Cr	Cu	Mn	Mo	N	Nb	Ni	P	S	Si	Ti	V
0.028	0.107	0.043	0.116	1.06	0.074	0.005	0.005	0.053	0.006	0.002	0.250	0.016	0.052

Table 2: Basic mechanical properties of the API grade X65 pipe material (base metal) and the weld metal determined with standardised methods. Weld metal values correspond to a heat input of 0.8 kJ mm^{-1}

	Yield strength (MPa)	Ultimate strength (MPa)	Area reduction (%)
X65 base metal	467 ± 10	570 ± 12	30
Weld metal 0.8 kJ mm^{-1}	581 ± 12	658 ± 14	10

Moreover, open source scripts are also available and allow the user to modify the algorithm that analyses the images. One popular method for analysing fluid dynamics is particle image velocimetry (PIV) that measures displacement fields in fluids based on pattern matching of successive images of a fluid with suspended particles. This technique is a generic tool for measuring displacements, and, in essence, it does not depend on whether images correspond to fluids or solids. Hence, it can be a useful tool for analysing the inhomogeneous deformation of solids as shown in the present study.

In this work, open libraries from the MATPIV project analysed the recorded images to calculate the strains. This project is an application of the PIV theory using MATLAB© scripts, in which the libraries are free under the terms of the GNU General Public License and the scripts are open. These libraries were useful in this study because they are available online, have tutoring information and are easily modified. Further details about pattern matching and libraries can be found in ref. [14].

Analysis of Images and Results

Straining experiments in the SEM consisted in the following steps: quasistatic loading of the specimen under constant cross-head speed, interrupting the loading, image capturing and resuming of loading until next strain level. Images with a resolution of 1536×1152 pixels and $50 \times$ magnification, which did not take long time to acquire, revealed a grid with sharp edges. Figure 4, which presents images recorded during the tensile tests of a 2.5 KJ mm^{-1} HAZ with the fusion line highlighted, showed that the weld metal underwent no apparent deformation while the HAZ suffered some stretching in the horizontal direction. The change in length in the axial direction of the squares provided an estimation of the engineering strain and showed that the maximum deformation reached by the HAZ was 12% at a load of (448 ± 4) N. Afterwards, the sample broke far from the fusion line because of problems in the grip. The HAZ with HI 0.8 KJ mm^{-1} produced similar images (not shown), but the maximum deformation achieved was only around 2%. In this case, the specimen broke in the base metal, implying that the HAZ with low HI presented a higher strength than the base metal.

PIV analysis

Although PIV is usually employed with random patterns, its theoretical bases are applicable to a regular grid such as the one previously shown. Thus, we had to evaluate the capabilities of the MATPIV algorithm to deal with the grid. The software proved accurate when displacements were smaller than the period of the grid, but it added spurious displacements when the values in the displacement field were closer to the period of the grid. The

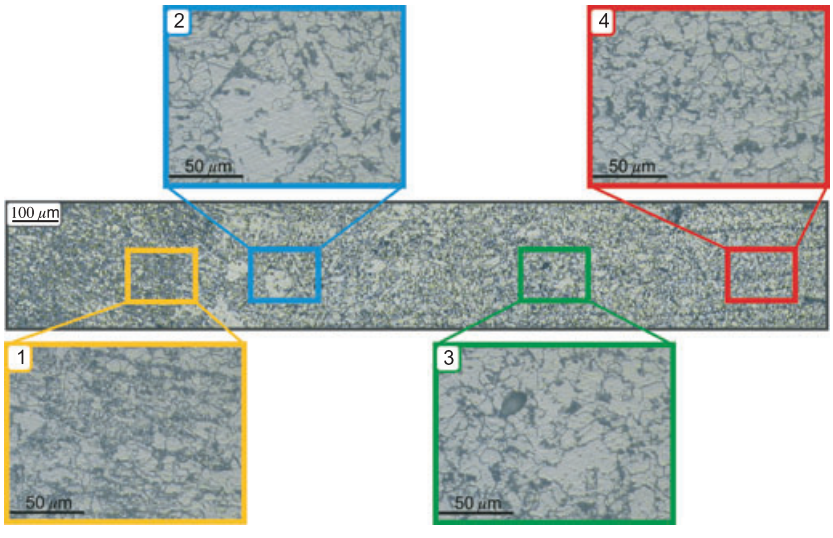

Figure 3: Microstructures of the high heat input HAZ. The fusion lines is between details 1 (weld metal) and 2 (CGHAZ). Notice the decrement in grain size from 2 to 4

doi: 10.1111/j.1475-1305.2010.00799.x

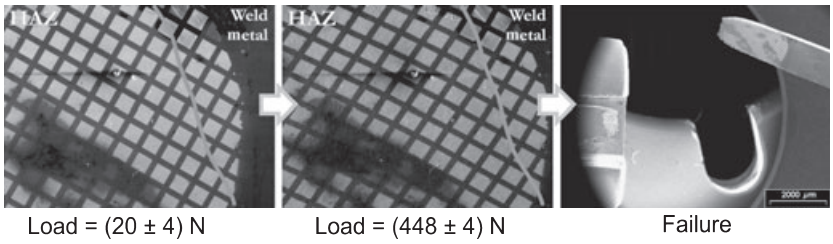

Figure 4: Images taken with the SEM during the test of a 2.5 KJ mm^{-1} HAZ. Compare the squares on the HAZ with those on the weld metal

problem disappeared when the number of pictures recorded increased, so displacements were smaller than the grid period, and results were further improved with *MATPIV* option 'multin'. This option starts the calculations with relatively large sub-windows and refines the results by using increasingly smaller windows (see [14] for further details). Based on trial and error, we selected a final window size (after refinement) of 192×192 pixels that led to a resolution in the displacement of 70 μm but maintained enough information in the sub-windows for adequately calculating the cross-correlation. The 'strain' subroutine in MATPIV calculated the strain fields using the option 'circulation' that was based on the Sobel's algorithm for recognising gradients.

Figure 5 is an example of the true strain field measured in the region between the weld metal and the HAZ with HI 2.5 KJ mm^{-1}. Notice how lateral contraction appears as white horizontal strips on the edges of this figure, which are most perceptible where the deformation is larger. Furthermore, transverse strains were around half the axial strain satisfying, within the experimental error, volume constancy. The figure shows that while the largest strains are visible within the HAZ, the weld metal seems to be almost unchanged. Using an average value of the strain for each HAZ sub-region and loads measured with the load cell, we estimated the strain–stress curve.

Stress–strain curves

The stress–strain curve of the CGHAZ material derived from the previous results by using an average value of the strain for each image came from the PIV analysis with the measured force. Thus, every image recorded in the *in situ* test corresponded to a point in the stress–strain diagram shown in Figure 6. Error bars in that figure resulted from combining the uncertainties in the measured load (that is negligible) and in the cross-sectional area of the specimen. Moreover, despite this work did not focus on an extensive analysis of errors from the PIV subroutine, we compared calculations with different sub-windows sizes and estimated an uncertainty in strain around 5% [15]. Then, the results showed that the strength of the 2.5 KJ mm^{-1} CGHAZ is 10% lower than that of the base metal, and the opposite occurred for the HI of 0.8 KJ mm^{-1}, in which the strength is about 10% higher than that of the base metal. The solid stress–strain curve belonged to a standardised test of the base metal while dotted lines corresponded to the values in Table 3 that belong to the notched specimen analysis discussed in the following section.

Strain localisation caused by material properties mismatch induces higher triaxiality on specimens [16] so it can affect stress values of *in situ* tests. This effect was quantified by applying the Bridgman model [17] with the curvature of the white horizontal stripes (lateral contraction) in

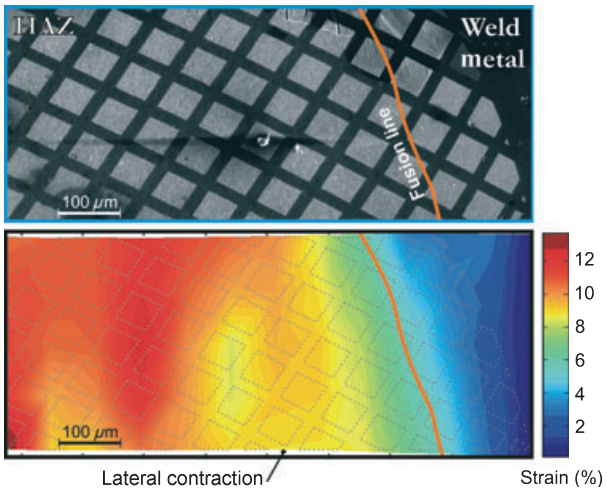

Figure 5: Measured axial strains for the tensile specimens. The full color picture is available on the online edition

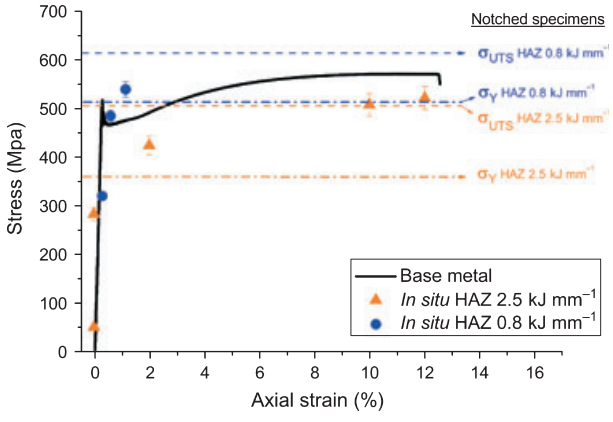

Figure 6: Stress–strain diagrams for the base metal and HAZ with different HIs

Table 3: Estimated yield and ultimate strength of HAZs with different HIs

HI kJ mm^{-1}	Yield strength, σ_Y (MPa)	Ultimate strength, σ_{UTS} (MPa)
HAZ 0.8	514 ± 39	615 ± 36
HAZ 2.5	360 ± 28	506 ± 28

doi: 10.1111/j.1475-1305.2010.00799.x

Figure 5. The calculations indicated that, using the smallest curvature measured, strain localisation increased stresses less than 2%, which is within the experimental error.

Comparison with Other Techniques

Hardness measurements

Hardness measurements are useful to compare and estimate a ranking for the strengths of the HAZ regions, weld metal, and base metal. As the relationship between hardness and strength is only an estimation that can depend on the underlying microstructure, the use of correlations between them is not conclusive (e.g. correlations for steel may have a standard error around 100 MPa [18], and they can depend on several parameters [19]). Figure 7 shows Vickers Hardness HV10 values obtained at different locations along the welds under study [20]. HAZ hardness values significantly differed for both HIs; for low HI, the shorter cooling time during the welding leads to higher hardness values and an expected higher tensile strength. On the contrary, for high HI the HAZ is significantly softer than the base metal and a lower tensile strength should be expected.

Notched bar tensile tests

To estimate the yield and the ultimate tensile strengths of the HAZ, this research also tested tensile specimens with a notch at the centre region of the weld (cap and root were removed). The notch, which had a radius of 0.25 mm, was located within the first millimeter of the HAZ, next to the fusion line, as shown in Figure 8A. Figure 8B presents the results obtained in the quasi-static tensile tests with notched specimens.

The following formulas for notched bar tests proposed in ref. [21] estimated the yield and the ultimate stresses as:

$$\sigma_Y = \frac{P_y}{C_Y \cdot \pi \cdot a} \tag{1}$$

$$\sigma_{UTS} = \frac{P_{UTS}}{C_{UTS} \cdot \pi \cdot a}, \tag{2}$$

in which P_Y and P_{UTS} are the yielding and the maximum loads respectively, a is the bar diameter at the notch and C_Y and C_{UTS} are constants that depend on specimen geometry. By assuming that constants do not depend on material properties, the comparison between the base metal tests of specimens with and without notches provided the values of the constants.

Table 3 presents the results for both HAZs showing that the HAZ with higher HI has significantly lower yield strength than the base metal. Even though these results agree with the hardness measurements, they are not conclusive because Equations (1) and (2) do not take into account the effect of inhomogeneity (e.g. higher induced triaxiality) that essentially implies that constants C_Y and C_{UTS} could vary with the specimen size or depend on the degree of mismatch. Moreover, this technique does not provide a rational methodology to estimate the uncertainties of the results.

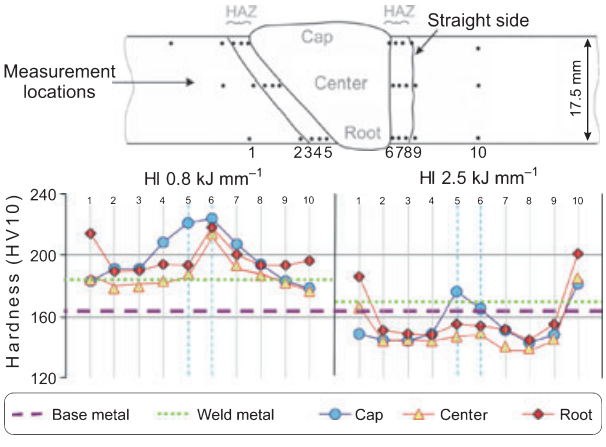

Figure 7: Hardness measurements at different locations along the HAZ region for HIs 0.8 and 2.5 kJ mm^{-1} [13]. Dashed and dotted lines indicate the hardness of the base and weld metals, respectively. Data numbered 4 and 7 correspond to the CGHAZ while those numbered 5 and 6 correspond to the fusion line

Discussion

Tensile tests of homogeneous materials usually result in narrow bands of uncertainty, but this is not the case for weld regions in which strong microstructural gradients lead to non-unique mechanical properties. The wide dispersion of properties increases the uncertainty and requires assessments to be more conservative, and thus suggests a need for a deeper understanding of the properties of the weld.

Hardness measurements showed significant differences among the HAZ, weld and base metals (Figure 7), but as mentioned before, any correlation of hardness with the tensile strength carries a significant error. Moreover, notched

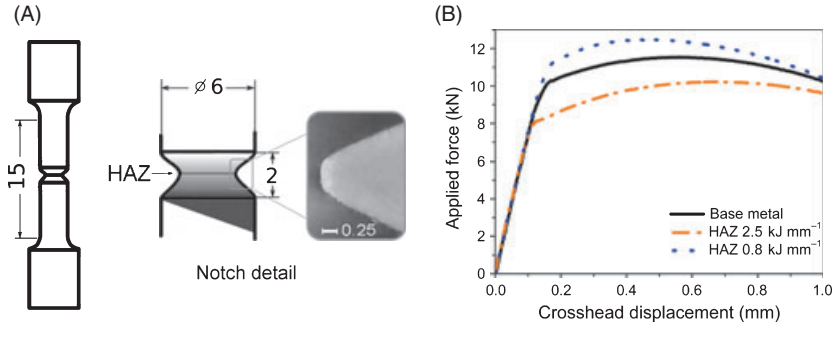

Figure 8: (A) Tensile tests notched specimens obtained from the centre part of the weld (cap and root were removed); dimensions are in millimeters. (B) Experimental results for notched specimens

doi: 10.1111/j.1475-1305.2010.00799.x

bar tests confirmed that the yield strength of the HAZ with higher HI was substantially lower than that of the base metal (Table 3). However, inhomogeneity induced triaxiality plays a role not considered in the model [Equations (1) and (2)], so more accurate results could only be obtained with finite elements simulations and detailed information of the weld metal strength. Because the previous techniques could not provide indisputable results of the HAZ tensile behaviour and no other well-stated methodology is available, this research developed an innovative solution. The proposed technique provided results of the HAZ tensile behaviour with well-defined uncertainties, which is a problem of technological interest not well solved yet. Moreover, despite the uncertainties in the results are not dazzling, they can be easily improved with better machined specimens and several PIV studies with different sub-window sizes that would allow a detail statistics quantification of the uncertainty.

One concern about the experimental methodology proposed is that the specimens were too thin to apply the results to the thicker pipeline. Micrographs showed that, in the worst case (i.e. the CGHAZ), the thickness of the specimens contained at least 25 grains, which is assumed to be sufficient to provide representative results. Moreover, a thin section turns to be beneficial because it makes the specimen closer to a plane stress state and decreases the triaxiality induced by the overmatching weld in one direction (in agreement with ref. [19]).

This work proposed a technique to characterise the local tensile behaviour in inhomogeneous materials and applied the technique to study the region of the HAZ next to the fusion line, the CGHAZ, but because of the wide magnification and depth of focus provided by the SEM, this technique is quite flexible for multi-scale analysis. The methodology has the potential to capture the behaviour of the entire HAZ by running one test in which images are recorded at different scales or taking just one picture with high definition. Then, only one specimen is required to measure the stress–strain curves of the different zones in the HAZ. Moreover, this methodology also allows the observation of strain localisation caused by material inhomogeneity, which could be a useful tool for validating constitutive models of HAZs.

Summary and Conclusions

The present study developed an innovative method to determine the local strength of inhomogeneous materials using mechanical tests inside a scanning electron microscope along with simple image correlation software, which was capable of measuring the tensile properties of the CGHAZ. Results agreed with indirect estimations such as hardness measurements and notched bar tests that could not provide indisputable results.

The open source code MatPIV successfully calculated displacements and strains of around 10% from the images of the *in situ* uniaxial tensile tests and exhibited a significant strain gradient located along the fusion line. Results showed that, for the steel pipe analysed, the strength of the HAZ of HI 2.5 KJ mm^{-1} was at least 10% lower than that of the base metal and 10% higher for 0.8 KJ mm^{-1}. The uncertainty of the results can be estimated accurately without assumptions on the material properties.

Finally, because of the capabilities of the SEM, *in situ* tests are quite flexible for multi-scale analysis, and when the SEM and PIV analysis are used together, they are capable of measuring the stress–strain behaviour at different regions in the HAZ and scales with one test.

ACKNOWLEDGMENTS

We gratefully acknowledge the support of the Comisión Nacional de Energía Atómica (CNEA) and CONICET, TENARIS SIDERCA and FUDETEC. The first author is particularly thankful for the feedback and support of Richard Bravo, the work on hardness measurements by Federico Daguerre and the technical assistance of Carlos Cotaro.

REFERENCES

1. DNV-RP-F108 Recommended Practice (2006) Fracture control for pipeline installation methods introducing cyclic plastic strain. *Det. Norske Veritas*. section 1.2.
2. Honeycombe, R. and Bhadeshia, H. K. (1995) *Steels: Microstructures and Properties*, 2nd edn. Edward Arnold, London: 291–301.
3. Kim, B. C., Lee, S., Kim, N. J. and Lee, D. Y. (1991) Microstructure and local brittle zone phenomena in high-strength low-alloy steel welds. *Metall. Trans. A*. **22**, 139–149.
4. BS 7910 (1999) *Guide on Methods for Assessing the Acceptability of Flaws in Fusion Welded Structures*. British Standard, London.
5. Zarzour, J. F., Konkol, P. and Dong, H. (1996) Stress–strain characteristics of the heat-affected zone in an HY-100 weldment as determined by microindentation testing. *Mater. Charact.* **37**, 195–209.
6. Chen, Y. T., Guo, A. M., Wu, L. X., Zeng, J. and Li, P. H. (2006) Microstructure and mechanical property development in the simulated heat affected zone of V treated HSLA steels. *Acta Metall. Sinica*. **19**(1), 57–67.
7. Loureiro, A. J. R. (2002) Effect of heat input on plastic deformation of undermatched welds. *J. Mater. Process. Technol.* **128**(1–3), 240–249.
8. Beghini, M., Bertini, L. and Di Puccio, F. (2001) Evaluation of mechanical properties of welded joints by small-specimen tests. *Strain* **37**, 155–158.
9. Mohr, W. (2006) Strain-based design: Strain concentration at girth welds. Draft final report (rev.1). EWI project no. 47447cap, EWI.
10. Molak, R.M., Paradowski, K., Brynk, T., Ciupinski, L., Pakiela, Z. and Kurzydlowski, K. J. (2009) Measurement of mechanical properties in a 316L stainless steel welded joint. *Int. J. Press. Vessels Pip.* **86**, 43–47.
11. Yawny, A., Malarría, J., Soukup, E. and Sade, M. (1997) Stage for in situ mechanical loading experiments in a scanning electron microscope (Philips 515) with a small chamber. *Rev. Sci. Instrum.* **68**(1), 150–154.
12. Biery, N., de Graef, M. and Pollock, T. M. (2003) A method for measuring microstructural-scale strains using a scanning electron microscope: applications to γ-titanium aluminides. *Metall. Trans. A*. **34**, 2001–2313.
13. Pisarski, H. G. (1996) TWI Research Report 566/1996. The Welding Institute, Abington Hall.

doi: 10.1111/j.1475-1305.2010.00799.x

14. Sveen, J. K. (2004) An Introduction to Matpiv v.1.6.1. Eprint No. 2, ISSN 0809-4403, Department of Mathematics, University of Oslo. Available at: http://www.math.uio.no/~jks/matpiv (last accessed 7 February 2010).
15. Hertzberg, R. (1996) *Deformation and Fracture Mechanics of Engineering Materials*, 2nd edn. Wiley, New York, NY.
16. Castelluccio, G. M. (2006) *Toughness of inhomogeneous materials: the heat affected zone in welds*. Master thesis, Instituto Balseiro (in Spanish).
17. Kim, Y. J. and Oh, C. S. (2006) Finite element limit analyses of under-matched tensile specimens. *Eng. Fract. Mech.* **73**(10), 1362–1378.
18. Pavlina, E. J. and Van Tyne, C. J. (2008) Correlation of yield strength and tensile strength with hardness for steels. *J. Mater. Eng. Perform.* **17**(6), 888–893.
19. Umemoto, M., Liu, Z. G., Tsuchiya, K., Sugimoto, S. and Bepari, M. M. A. (2001) Relationship between hardness and tensile properties in various single structured steels. *J. Mater. Sci. Technol.* **17**, 505–511.
20. Daguerre, F. (2006) *Private Communication*. Tenaris, Tenaris Internal Report, Campana, Buenos Aires, Argentina.
21. Valiente, A. and Lapeña, J. (1996) Measurement of the yield and tensile strengths of neutron-irradiated and post-irradiation recovered vessel steels with notched specimens. *Nucl. Eng. Des.* **167**, 11–22.

doi: 10.1111/j.1475-1305.2010.00799.x